Method to obtain g-functions for multiple precast quadratic pile heat exchangers

Pagola, Maria Alberdi; Jensen, Rasmus Lund; Madsen, Søren; Poulsen, Søren Erbs

Publication date:
2018

Document Version
Publisher's PDF, also known as Version of record

DEPARTMENT OF CIVIL ENGINEERING
AALBORG UNIVERSITY

Method to obtain g-functions for multiple precast quadratic pile heat exchangers

Maria Alberdi-Pagola
Rasmus Lund Jensen
Søren Madsen
Søren Erbs Poulsen (VIA University College, Horsens)

ISSN 1901-726X
DCE Technical Report No. 243

Aalborg University
Department of Civil Engineering
Group Name

DCE Technical Report No. 243

Method to obtain g-functions for multiple precast quadratic pile heat exchangers

by

Maria Alberdi-Pagola
Rasmus Lund Jensen
Søren Madsen
Søren Erbs Poulsen (VIA University College, Horsens)

May 2018

Scientific Publications at the Department of Civil Engineering

Technical Reports are published for timely dissemination of research results and scientific work carried out at the Department of Civil Engineering (DCE) at Aalborg University. This medium allows publication of more detailed explanations and results than typically allowed in scientific journals.

Technical Memoranda are produced to enable the preliminary dissemination of scientific work by the personnel of the DCE where such release is deemed to be appropriate. Documents of this kind may be incomplete or temporary versions of papers—or part of continuing work. This should be kept in mind when references are given to publications of this kind.

Contract Reports are produced to report scientific work carried out under contract. Publications of this kind contain confidential matter and are reserved for the sponsors and the DCE. Therefore, Contract Reports are generally not available for public circulation.

Lecture Notes contain material produced by the lecturers at the DCE for educational purposes. This may be scientific notes, lecture books, example problems or manuals for laboratory work, or computer programs developed at the DCE.

Theses are monograms or collections of papers published to report the scientific work carried out at the DCE to obtain a degree as either PhD or Doctor of Technology. The thesis is publicly available after the defence of the degree.

Latest News is published to enable rapid communication of information about scientific work carried out at the DCE. This includes the status of research projects, developments in the laboratories, information about collaborative work and recent research results.

Published 2018 by
Aalborg University
Department of Civil Engineering
Thomas Manns Vej 23
92200 Aalborg East, Denmark

Printed in Aalborg at Aalborg University

ISSN 1901-726X
DCE Technical Report No. 243

Recent publications in the DCE Technical Report Series

The present report complements a series of technical reports:

Alberdi-Pagola, M., Poulsen, S. E., Jensen, R. L., & Madsen, S. (2017). Thermal response testing of precast pile heat exchangers: Fieldwork report. Aalborg: Aalborg University. Department of Civil Engineering. DCE Technical Reports, No. 234.

Alberdi-Pagola, M., Jensen, R. L., Madsen, S., & Poulsen, S. E. (2017). Measurement of thermal properties of soil and concrete samples. Aalborg: Aalborg University. Department of Civil Engineering. DCE Technical Reports, No. 235.

Contents

Introduction

The average fluid temperature circulating through the ground loop is one of the main parameters required when choosing the most adequate heat pump for a ground source heat pump installation. Besides, the analysis of the fluid temperature over time will show the sustainability of the energy supply over the lifetime of the installation. The average fluid temperature is subjected to the type of ground heat exchangers and the thermal interactions between them, which also depend on the soil thermal properties. For the case of precast piles, the thermal interactions become significant as they are usually placed within short distances (0.5 to 4 metres). Fast models that can account for these interactions are required to enable feasibility studies and support the design phase. Besides, since pile heat exchangers have a main structural role, it is also relevant to develop models that can determine the temperature changes that the foundation might be subjected to, to assess thermo-mechanical implications.

3D finite element model (FEM) computation of the thermal behaviour of multiple pile heat exchanger foundations is not cost effective nor for feasibility studies, nor for most design applications. Therefore, this report describes a method to obtain simpler semi-empirical models based on 3D FEM simulations, called multiple pile g-functions.

The precast quadratic cross section pile heat exchangers analysed in this report have single-U and W-shape pipe heat exchangers and their aspect ratios (AR = Length/Diameter) are limited to 15, 30, 45 and 53. They are further described in [1] and [2]. The proposed g-functions account for the transient heat storage within the pile and are applicable over a range of timescales up to 20 years. This report builds on the methodology described in [3,4] and uses a similar notation. Different g-functions are used to describe the temperature responses of the ground surrounding the pile (ground G-functions G_g) and of the pile itself (concrete G-functions G_c).

The report first defines the g-functions, and then it explores each element required for the calculation of the average fluid temperature. After, some examples are studied, and an error analysis derived from using simplifications in the model is performed before the model is applied to analyse field thermal response test (TRT) data.

G-functions: definitions

The average fluid temperature T_f [°C] circulating through the ground-loop is one of the main parameters required to choose the most adequate heat pump for a ground source heat pump installation. The average fluid temperature T_f can be defined as:

$$T_f = T_0 + \frac{q}{2\pi\lambda_s} G_g + qR_c G_c + qR_{pipe} \quad (1)$$

Where T_0 [°C] is the undisturbed soil temperature, q [W/m] is the heat transfer rate per metre length of pile heat exchanger, λ_s [W/m/K] is the thermal conductivity of the soil, G_g is the g-function describing the ground temperature response, R_c [K·m/W] is the steady state concrete thermal resistance, G_c is the concrete g-function describing the transient concrete response and R_{pipe} [K·m/W] is the thermal resistance of the pipes. In the following, each term of Equation 1 will be analysed.

G-functions are dimensionless response factors that describe the change in temperature in the ground around a heat exchanger with time as a result of an applied thermal load q [5]. Usually, both temperature change and time are normalised. In this study, the normalised temperature changes Φ and time Fo are defined as:

$$\Phi = \frac{2\pi\lambda_s \Delta T}{q} \quad (2)$$

$$Fo = \frac{\alpha_s t}{r_b^2} \quad (3)$$

where ΔT [K] is the temperature change between the undisturbed soil temperature T_0 [°C] and the average pile wall temperature T_b [°C], α_s [m^2/s] is the thermal diffusivity, i.e., the ratio between the thermal conductivity λ_s [W/m/K] and the volumetric heat capacity of the soil ρc_{ps} [J/m^3/W], t [s] is the time and r_b [m] is the pile equivalent radius. The pile radius is the radius that provides an equivalent circumference to the square perimeter.

G-functions are used to calculate the pile wall temperature. For a single pile, the pile wall temperature depends on time and its aspect ratio ($L/2r_b$), and it can be determined as:

$$T_b = T_0 + \frac{q}{4\pi\lambda_s} \cdot G(Fo, \frac{L}{2r_b}) \quad (4)$$

G-functions can be obtained by analytical, numerical and empirical methods. The pile g-functions presented in this study are semi-empirical models based on 3D FEM of a single pile heat exchanger,

where temporal and spatial superposition techniques ease the consideration of the thermal influence between piles.

Single pile G-function G_g

The methods to obtain single pile g-functions are given before the simulation results are analysed.

Methods

The ground temperature response functions G_g, or single pile G-functions, are based on 3D numerical analyses and are valid for time ranges $0.1 < Fo < 10000$. These functions describe the time dependent pile wall temperature evolution under a constant thermal load. As this temperature response will be affected by the surface boundary, i.e., it will be affected by the length of the pile heat exchanger, different pile aspect ratios AR have been considered. Based on the most common produced precast piles, aspect ratios of 15, 30, 45 and 53 and single-U and W-shape pipe arrangements have been considered. The numerical models were constructed using the software COMSOL Multiphysics [6] and they comprise a full representation of the pile, the built-in pipes and the surrounding soil (Figure 1).

The model contains the ground surrounding the pile up to a radial distance of 25 m and beneath the base of the pile to 25 m. The soil and concrete properties used in the model are given in Table 1. The properties are assumed constant with temperature changes due to the relatively small temperature changes related to energy geostructure applications. The radial outer, top and base boundaries are kept at a constant temperature of 10 °C. The initial temperature is set to 10 °C everywhere in the model and groundwater flow was neglected.

Model tests were made to ensure that the modelled temperatures are independent to the chosen temporal and spatial discretisation. The mesh is refined in the immediate vicinity of the pile, it expands towards the model outer boundary and it comprises tetrahedral, prismatic, triangular, quadrilateral, linear and vertex elements. The models have been verified in [1].

To guarantee the maintenance of a specific heat injection rate [W/m], an inlet temperature history was dynamically generated during the simulation by coupling the inlet to the outlet temperature of the previous time step. The water flow is ensured turbulent. 20-year simulations are performed. The temperature response at the pipe boundary, at the edge of the pile and the soil are recorded by the model.

Table 1: Properties of the materials used in the models.

Parameters [units]	Values
Volumetric heat capacity concrete ρc_{pc} [MJ/m^3/K]	2.00
Thermal conductivity concrete λ_c [W/m/K]	2.00
Volumetric heat capacity soil ρc_{ps} [MJ/m^3/K]	2.00
Thermal conductivity soil λ_s [W/m/K]	1.00, 2.00, 4.00
Thermal conductivity pipe λ_{pipe} [W/m/K]	0.42

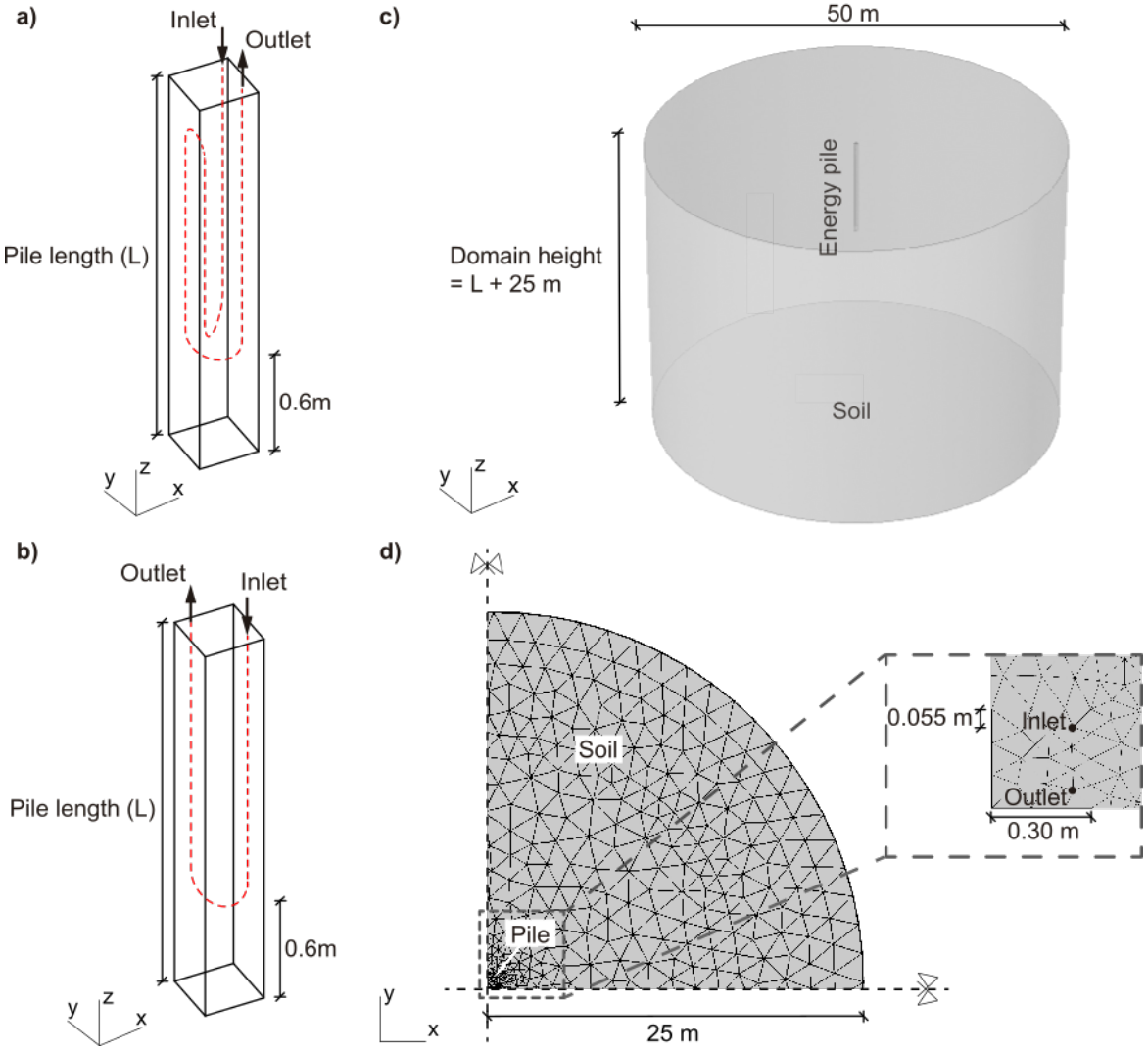

Figure 1: Description of the 3D finite element model: a) schematic of the W-shape pile heat exchanger; b) schematic of the single-U pile heat exchanger; c) simulated domains; d) top view of a quarter domain.

To sum up, the following assumptions have been considered for the derivation of the model:

- The ground is regarded as homogeneous medium and its thermo-physical properties do not change with temperature.
- The medium has a uniform initial temperature.

- The heating rate per unit length is constant from the starting instant.
- A constant ground surface temperature has been imposed.
- No heat convection due to groundwater flow has been considered.
- The steel reinforcement is not modelled since it has not a significant effect on the overall thermal performance of the pile [7].

Simulation results

A common way to show the temperature response factors in literature, is by computing the dimensionless temperature Φ over time Fo as a result of a constant thermal load, i.e., resembling a long thermal response test. Based on simulated average temperatures around the pile perimeter, a summary of the model ground temperature responses G_g are presented in Figure 2. A range of curves is possible depending on the aspect ratio AR, the size of the pile and the relative properties of the pile concrete and the surrounding ground. Figure 2 depicts the cases where the thermal conductivities of soil λ_s and concrete λ_c are the same.

For easier implementation of the temperature response functions G_g curve fitting has been carried out for the G-functions presented in Figure 2, in a similar way to the process followed by [3,8]. The results are contained in Appendix A.

The impact of the concrete thermal conductivity λ_c will be taken into account by consideration of the relative conductivities of the ground and the concrete (λ_c/λ_s) in the temperature response of the pile concrete itself, which is discussed in the next section.

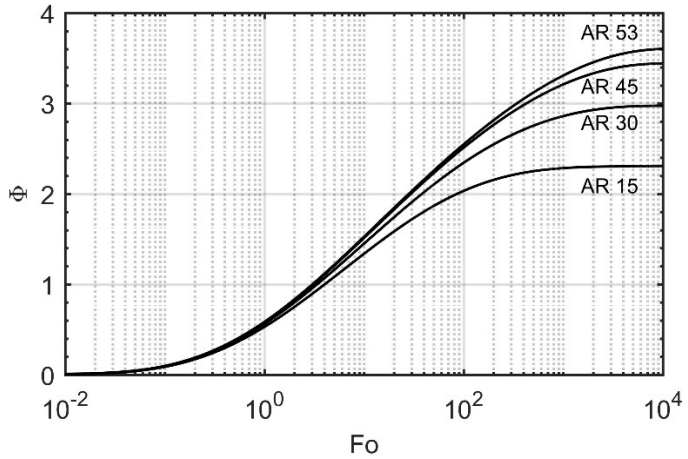

Figure 2: Pile G-functions for precast pile heat exchangers with different aspect ratios (AR) 15, 30, 45 and 53.

Concrete G-functions G_c

First, the method to obtain the transient concrete G-function G_c is described and simulation results are analysed afterwards.

Methods

The concrete G-function, as defined by [3,9], describes the transient thermal resistance of the pile heat exchangers. It depends on the shape of the pile cross section, the position of the pipes and the thermal conductivity of the concrete λ_c. That is, it defines the thermal resistance of the concrete part. To incorporate the transient response of the pile concrete into the overall temperature response function (Equation 1), the proportion of the steady state thermal resistance that has been achieved at a given value of time Fo has been calculated using the temperature field output from the 3D FEM. Ref. [1] demonstrated that 96% of the steady state in the concrete is reached by 100 hours (Fo ≈ 10). The thermal resistance of the concrete part of the pile is calculated over time as:

$$R_c = \frac{T_p - T_b}{q} \tag{5}$$

where T_p [°C] is the average temperature on the outer wall of the pipe.

Simulation results

The steady state resistance is the asymptotic value of Equation 5 calculated at large values of time, when Fo approaches 1000 [3]. It can be calculated numerically, as it was done in [1], for different pipe arrangements and a range of concrete thermal conductivities λ_c. As presented in [1], the aspect ratio of the pile does not considerably affect the concrete thermal resistance R_c. Figure 3a shows the most conservative cases. The range of laboratory measurements of the thermal conductivity of the concrete λ_c, reported in [1,10], have been added. This limits the concrete thermal resistances to a narrower range.

The proportion of the steady state value of the concrete thermal resistance R_c is shown in Figure 3b for single-U and W-shape piles. The case for $\lambda_c/\lambda_s = 1$ is shown. Curves for different λ_c/λ_s ratios (0.5 and 2) are given in the corresponding Appendix C.

To allow the calculation of the steady state R_c values and to ease the implementation of the response curves as concrete G-functions, curve fit data are presented in Appendix B and Appendix C, respectively.

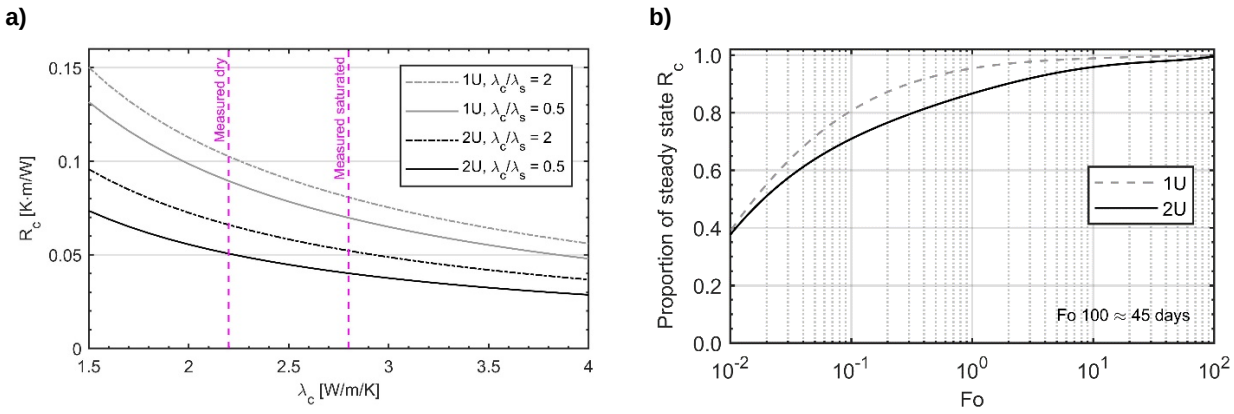

Figure 3: a) Upper and lower bounds for the steady state concrete thermal resistance R_c for square precast pile heat exchangers for 30x30 cm² with single-U (1U) and W-shape (2U) pipes obtained from 3D FEM modelling for a range of concrete thermal conductivities, after [1]**. b) Proportion of steady state R_c for time for single-U (1U) and W-shape (2U) piles.**

Pipe thermal resistance R_{pipe}

The method to obtain the pipe thermal resistance is shortly described before an analysis of the results is given.

Methods

The heat exchanger pipes pose an obstacle for the heat to be dissipated from the circulating fluid towards the pile and the soil and vice versa. Thus, a pipe thermal resistance needs to be considered. The heat transfer process within the pipes will reach steady state rapidly and, hence, the pipe thermal resistance is considered constant. The pipe thermal resistance R_{pipe} [K·m/W] is defined in Equation 6 as the sum of the pipe convective (first term on right hand side) and conductive (second term on right hand side) resistances:

$$R_{pipe} = \frac{1}{2n\pi r_i h_i} + \frac{\ln(r_o/r_i)}{2n\pi\lambda_{pipe}} \quad (6)$$

where n is the number of pipes in the pile heat exchanger cross section, r_i [m] is the inner radius of the pipe, r_o [m] is the outer radius of the pipe, h_i [W/m²/K] is the heat transfer coefficient and λ_{pipe} [W/m/K] is the thermal conductivity of the pipe material. h_i can be calculated using the Gnielinski correlation as described in [11,12].

Results

The pipe thermal resistances for different pipe configurations (single-U and W-shape) and different pipe diameters Ø are shown in Figure 4 for a range of Reynolds numbers. The Reynolds number is

a dimensionless quantity that establishes whether a circulating fluid flows at laminar, transient or turbulent regime [11,12]. The pipe thermal resistance significantly decreases in the change from laminar to turbulent flow. However, it does not meaningfully improve once turbulence is reached.

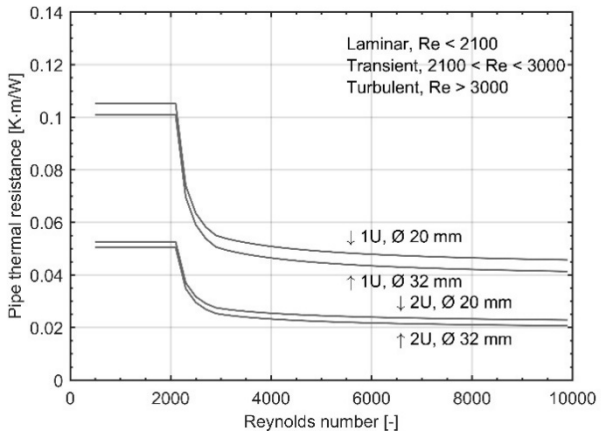

Figure 4: Pipe thermal resistance VS Reynolds number for different pipe arrangements and pipe diameters Ø.

Multiple pile g-functions

First, the methods to obtain multiple pile g-functions are described and simulation results are analysed afterwards.

Methods

The multiple pile heat exchanger g-functions are based on the temperature fields extracted from the 3D FEM described in the section “Single pile G-functions G_g” and in Figure 1. The simulations are used to obtain, in addition to the pile wall temperature, soil temperatures at required radial distances, r = S [m], that would resemble pile spacing.

The multiple pile g-functions provide the change in the average pile wall temperature over time of all the piles comprising the foundation. I.e., the g-function gives the pile wall temperature for a specific foundation configuration due to a constant heat input rate [13]:

$$T_b = T_0 - \frac{q}{4\pi\lambda_s} \cdot g(Fo, \frac{L}{2r_b}, \frac{S}{2r_b}) \quad (7)$$

where T_b [°C] is the pile wall temperature common to all piles, T_0 [°C] is the undisturbed ground temperature, q [W/m] is the average heat extraction rate per pile length, λ_s [W/m/K] is the ground thermal conductivity, g is the multiple pile g-function. For the case of pile heat exchanger foundations or groups, the multiple g-functions depend on three non-dimensional parameters: the dimensionless time, the AR ($L/2r_b$), being L [m] the active length of the pile heat exchanger and the foundation aspect ratio $S/2r_b$, being S the centre to centre pile spacing, as defined in [4].

For various piles, the g-function can be calculated by applying temporal and spatial superposition of the single pile G-function and radial temperatures. This principle relies on the heat conduction equation and boundary conditions on being linear [13].

In the spatial superposition the temperature distributions around every ground heat exchanger are added in order to calculate the overall temperature variation at the pile walls [14]:

$$\Delta T_b(t) = \frac{1}{n_p}\sum_{i=1}^{n_p}\sum_{j=1}^{n_p}\Delta\overline{T}(d_{ij}, t) \tag{8}$$

$$d_{ij} = \begin{cases} r_b, & i = j \\ \sqrt{(x_i - x_j)^2 + (y_i - y_j)^2}, & i \neq j \end{cases} \tag{9}$$

where ΔT_b [K] is the average temperature variation at the pile heat exchanger wall, (x_i, y_i) [m] are the coordinates of the i^{th} pile heat exchanger, n_p is the number of pile heat exchangers in the foundation and d_{ij} [m] is the pile distance.

Time variations can be applied by deconvolution of the time varying heat transfer rate [13]. The temperature at discrete time step in the pile heat exchanger foundation is computed as:

$$\Delta T_n = \sum_{i=1}^{i=n}\frac{q_i}{2\pi\lambda_s}\left(G\left(Fo_n - Fo_{(i-1)}\right) - G(Fo_n - Fo_i)\right) \tag{10}$$

In an energy foundation, the pile heat exchangers can be connected in series and/or in parallel. This study analyses pile heat exchangers connected in parallel. This has an impact on the temperatures that develop around each individual heat exchanger. It is assumed that the heat extraction rates are uniform and equal for all the energy piles. As a result of this boundary condition, identified as boundary condition BC I in [15], the average temperatures along the length of all the piles are unequal. Hence, the average of the mean pile wall temperatures is used in the evaluation of the g-function.

Simulation results

Radial soil temperatures

Based on simulated average soil temperatures at increasing radial distances S from the pile centre, a summary of the dimensionless ground temperature responses Φ plotted against normalised time Fo are presented in Figure 5. The uppermost curve corresponds to the earlier described single pile G-function (Figure 2) as it represents the pile wall temperature. The rest of the curves correspond to

increasing normalised radial distances, from top to bottom, i.e., the bigger the distance, the smaller the thermal influence.

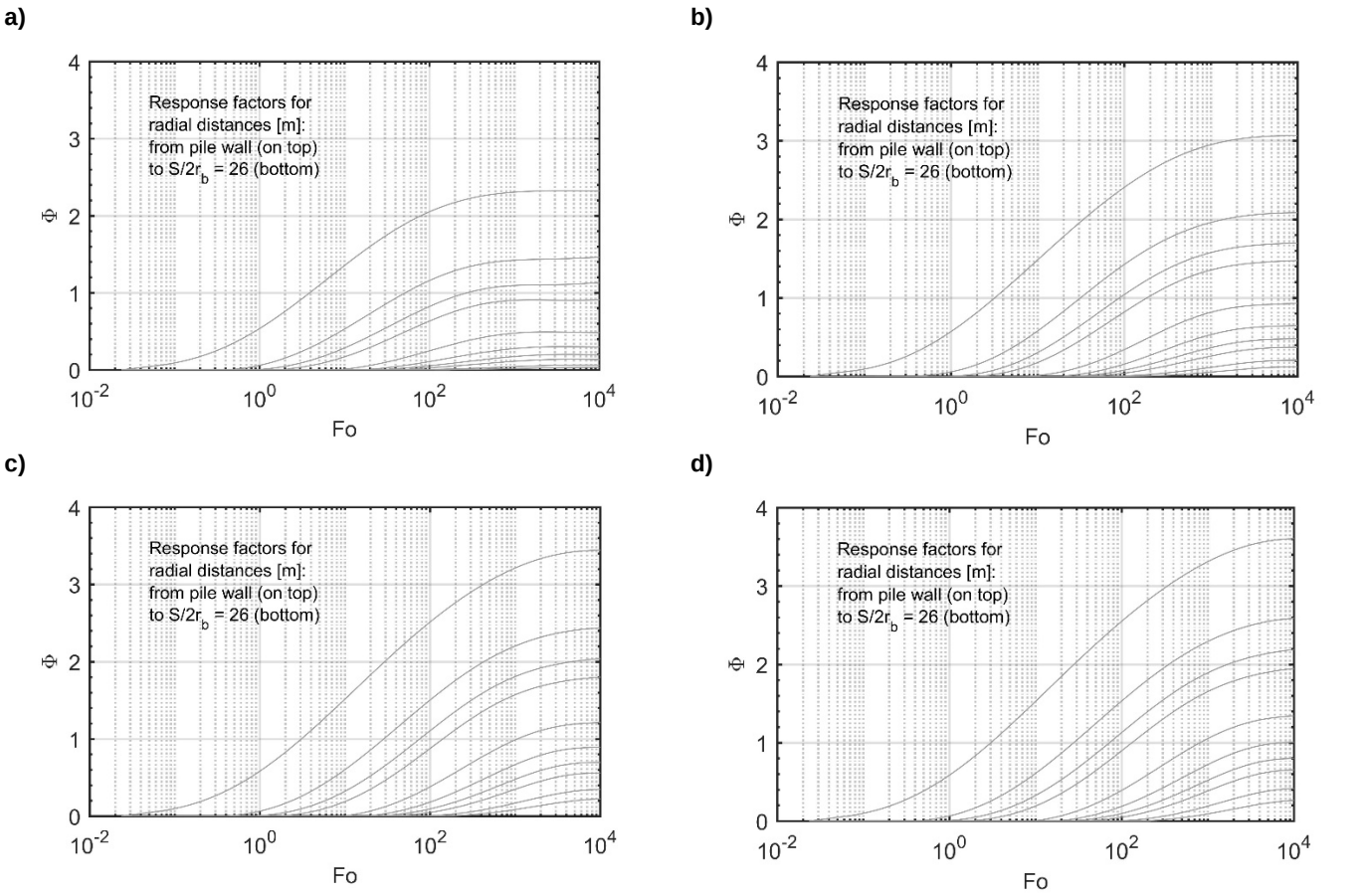

Figure 5: Dimensionless temperature responses for soil temperature changes at normalised distances $S/2r_b = T_b$, 1.3, 2, 2.6, 5.2, 7.9, 10.5, 13.1, 19.6, 26: a) aspect ratio 15; b) aspect ratio 30; c) aspect ratio 45; d) aspect ratio 53.

To ease the implementation, empirical equations for the curves have been calculated. The curve fitting parameters are provided in the corresponding Appendix D. For values of AR and distances that are not considered in the tables of coefficients, a linear interpolation needs to be applied to obtain the g-functions. Linear interpolations are considered sufficient precise and quick [8]. This issue is further described in the following section “Error analysis”.

The curves provided in Figure 5 can be superimposed in time and space to account for multiple piles. A thorough analysis of two interacting piles is used to analyse the main implications on the response factors [4]. Figure 6 reproduces the influence of the aspect ratio for several pile spacings: i) the closer the piles, the greater the temperature changes at steady state; ii) the higher the aspect ratio, the greater the degree of interaction between piles. Piles with higher aspect ratios have a higher overall temperature change and they influence a further distance in the ground due to the later influence of the surface boundary, in contrast to the piles with lower aspect ratios. Therefore, low aspect ratio piles might be more efficient.

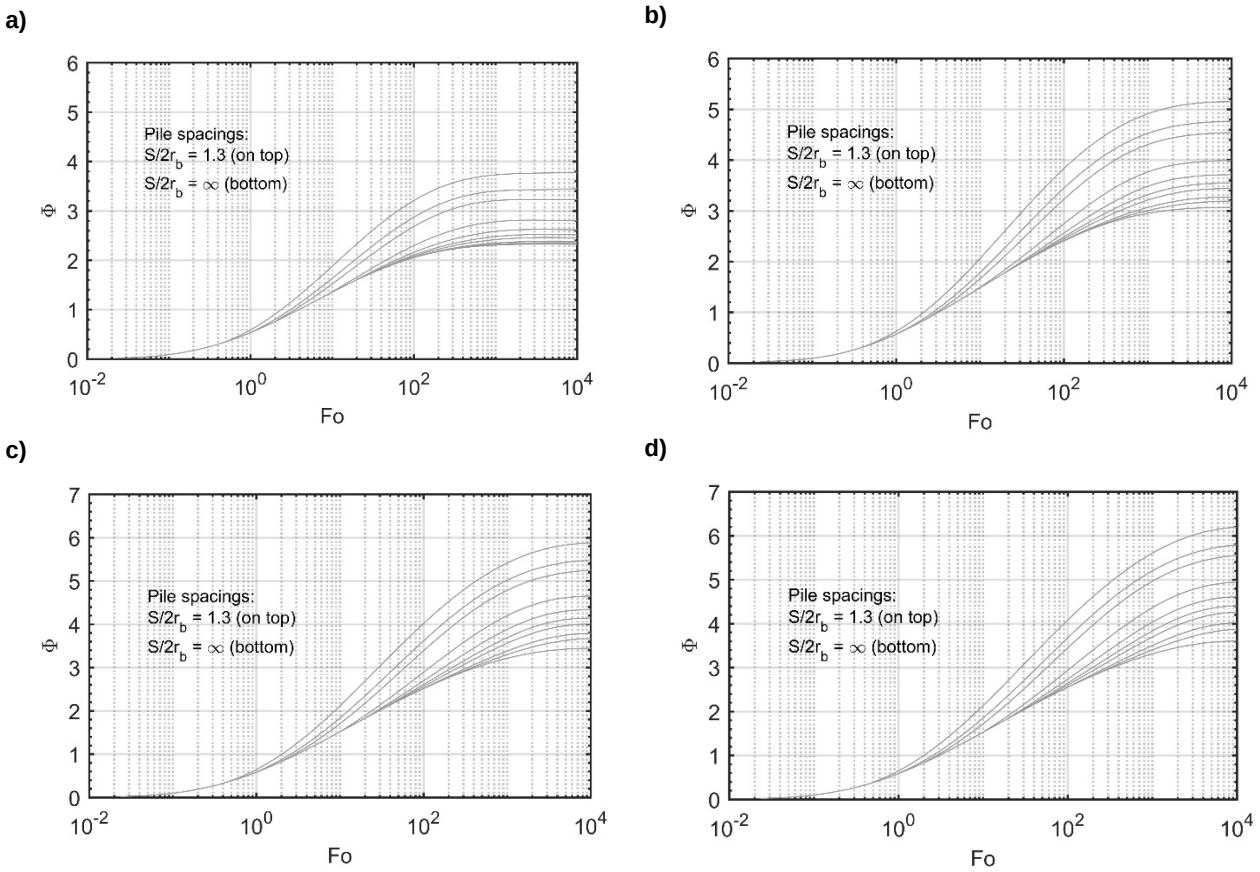

Figure 6: Response factors for two interacting piles at pile spacings $S/2r_b$ = 1.3, 2, 2.6, 5.2, 7.9, 10.5, 13.1, 19.6, 26.2, ∞ (= single pile); a) aspect ratio 15; b) aspect ratio 30; c) aspect ratio 45 and d) aspect ratio 53.

Figure 7 plots the percentage increase of the dimensionless temperature Φ with normalised distance $S/2r_b$ for normalised times Fo equal to 0.1, 1, 10, 100, 1000 and 10000. The interactions are mild at small values of time regardless of the pile spacing and pile geometry. However, as time increases, larger aspect ratio piles interact more and for longer.

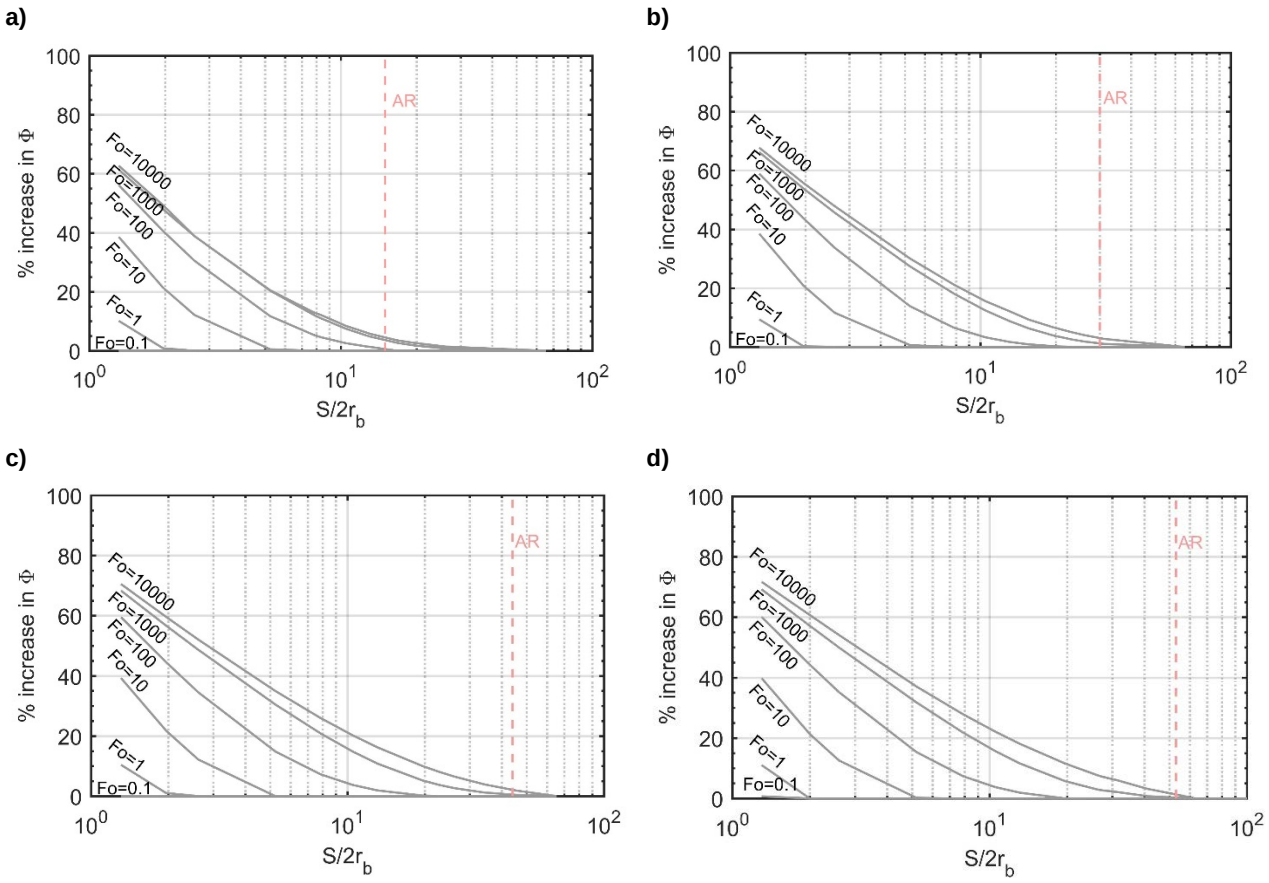

Figure 7: Percentage increase in dimensionless temperature for different normalized pile spacings; a) aspect ratio 15; b) aspect ratio 30; c) aspect ratio 45; d) aspect ratio 53.

It is assumed that there is no interference between borehole heat exchangers if the borehole spacing is bigger than its length and interactions are small for spacings half the length [5]. Loveridge and Powrie [4] defined that for pile heat exchangers, that criterion is equivalent to $S/2r_b > AR$. For a pile heat exchanger foundation, where the pile positions and spacings are governed by structural and geotechnical requirements of the building, interaction will happen since the minimum pile spacing will be lower than 5 m, for the case of precast pile heat exchangers.

Representative foundation patterns

Specific regular patterns (listed in Table 2) for pile aspect ratio 45 have been selected to investigate multiple pile g-functions with different pile spacings.

Table 2: Selected pile heat exchanger field configurations.

Pile arrangement	Pile spacing S [m]
1x2	1, 3, 5
1x3	1, 3, 5
2x3	1, 3, 5
2x4	1, 3, 5
3x3	1, 3, 5
4x4	1, 3, 5

Figure 8 shows g-functions in the form of non-dimensional curves Φ and the significant impact that multiple pile heat exchangers can have when interacting is illustrated for aspect ratio 45. For a single pile, i.e., when the pile spacing approaches infinity, the long term steady state normalized temperature response is approximately 3.4. For two piles at 1 m, the response increases to 5, for three piles and sixteen piles at the same spacing is 6.5 and 21.5, respectively. These increases will result in a corresponding decrease in the energy that can be exchanged per linear metre of the pile, as demonstrated in [4].

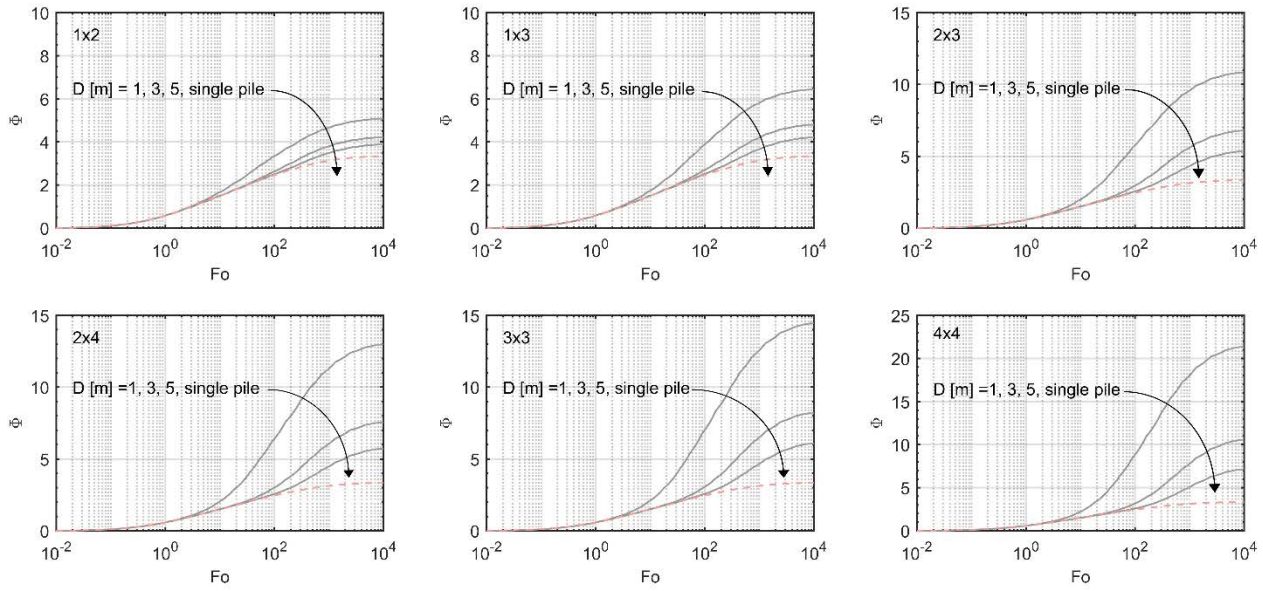

Figure 8: Multiple pile g-functions for different pile arrangements for aspect ratio AR 45 pile heat exchangers. The red dashed line represents the single pile g-function, i.e., an infinite pile spacing.

Table 3 summarises the increase in dimensionless temperature Φ for spacings of 1, 3 and 5 m and Table 4 provides the energy output percentage for different pile arrangements compared to a single pile. It is highlighted that at steady state with six piles in a 2x3 grid, each pile is only delivering 31% of the energy of an individual isolated pile.

For the case of precast piles, it is common to drive them in clusters, sometimes placed at distances below 1 m. In the case that all piles are equipped as pile heat exchangers, this would lead to an increase of the interactions, what is detrimental for the installation. It may be more cost-effective to equip only some of these piles with heat transfer pipes.

Table 3: Steady state increase in Φ for different pile arrangements compared to a single pile (AR = 45).

Pattern / Spacing	Single pile	1x2	1x3	2x3	2x4	3x3	4x4
1 m	-	52	93	225	290	334	542
3 m	-	26	44	104	127	147	217
5 m	-	17	26	61	72	83	114

Table 4: Energy output [%] for different pile arrangements compared to a single pile (AR = 45).

Pattern / Spacing	Single pile	1x2	1x3	2x3	2x4	3x3	4x4
1 m	-	66	52	31	26	23	16
3 m	-	79	69	49	44	41	32
5 m	-	86	79	62	58	55	47

Limitations of the model

There are several error sources when developing the semi-empirical multiple pile g-functions and that will affect its accuracy. There are errors derived from: i) fitting polynomials to the raw 3D FEM data; ii) interpolating between distances where data is not given; iii) simplifying the pile to a point without considering its volume.

The errors derived from the polynomial simplification are minimal, as it can be checked in the goodness of fit available in the appendix tables. I.e., the errors derived from the data fit for the selected distances extracted from the single pile with soil 3D FEM model are low.

The main errors are expected to come from the spatial interpolation, for pile spacings where raw data are not available. Tables 5 and 6 show the errors derived from using interpolation and the sensitivity of the error to the type of interpolation (linear or cubic). Here, the last time step of the multiple pile g-function is compared for the 4x4 pattern with 1 and 3 m pile spacings.

Table 5: g-function value for the 4x4 pattern with 1 m pile spacing.

Type of interpolation	Interpolated g-function	No-interpolated g-function	Error [%]
Linear	22.3	21.7	2.6
Cubic	22.1		1.8
Error [%]	0.9	-	

Table 6: g-function value for the 4x4 pattern with 3 m pile spacing.

Type of interpolation	Interpolated g-function	No-interpolated g-function	Error [%]
Linear	11.0	10.7	2.5
Cubic	10.9		1.7
Error [%]	0.9	-	

The errors assigned to the spatial interpolation are small for the purpose of this study, around 2.5%. Hence, linear interpolation is assumed acceptable, yet cubic interpolation is advised. However, it needs to be considered that these errors will accumulate as the amount of piles increases. The inaccuracies derived from these errors will be analysed in a journal paper, where the discrepancies between the temperatures computed with the proposed g-functions and full 3D finite element models of multiple piles will be discussed.

Besides, the model has the following limits:

- It does not account for the case of groundwater flow.
- It is applicable when soil stratification does not affect thermal properties significantly.
- It does not account for heat gains/losses from surface, such as heat gains from the building or solar gains.

Interpretation of TRT data

Once all the terms are analysed, the average fluid temperature in the ground-loop is calculated following Equation 1. To explore the applicability of these semi-empirical models, interpretation of precast pile heat exchanger TRT data has been performed.

Methods

The analysed precast pile heat exchanger TRT data are available in [16]. The inverse modelling approach is the same as described in [1]: the parameter estimation is performed with PEST [17] and the model is based on Equation 1, from where the inverse modelling yields estimates of the thermal conductivity of the soil λ_s [W/m/K] and the steady state concrete thermal resistance R_c [Km/W].

Results

Five TRTs have been analysed: LM1 corresponds to a single-U pile heat exchanger while the other four have a W-shape pipe arrangement. The results are compared to the 3D FEM calibration estimates reported in Table 5 in [1]. Figure 9 shows the parameter estimates normalised by the 3D FEM results.

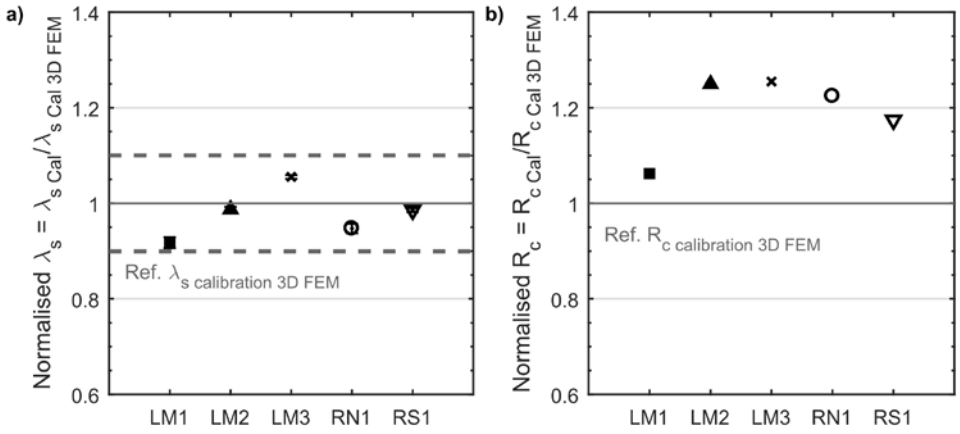

Figure 9: Parameter estimates from calibration of the semi-empirical models normalised by the 3D EFM based estimates. a) Thermal conductivity of soil λ_s; the uncertainty bounds correspond to the largest uncertainty obtained in the calibration of the 3D FEM models (test RN1); b) Concrete thermal resistance; uncertainties are not shown as they are insignificant (order of 10^{-2} Km/W). LM1: single-U. LM2, LM3, RN1 and RS1: W-shape.

The semi-empirical models provide a reliable estimation of the thermal conductivity of the soil λ_s. However, they tend to overestimate the concrete thermal resistance R_c by 20% and 6% for the W-shape and single-U piles, respectively. The proposed models show acceptable results and can be used for TRT interpretation.

Conclusions

This report presented in detail the methodology to obtain multiple precast pile heat exchanger g-functions, its different parameters, errors and applications. It has been demonstrated that this energy pile heat flux model is able to yield acceptable estimates of thermal conductivity of the soil λ_s [W/m/K] and pile concrete thermal resistance R_c [Km/W], when is used to interpret thermal response test data. The proposed method allows a fast assessment of the ground-loop fluid temperatures.

The polynomial expressions presented in this report will be compared to multiple pile 3D finite element models in a journal paper, where their suitability will be assessed, and the nature of the discrepancies will be discussed.

References

[1] M. Alberdi -Pagola, S.E. Poulsen, F. Loveridge, S. Madsen, R.L. Jensen, Comparing heat flow models for interpretation of precast quadratic pile heat exchanger thermal response tests, Energy. 145 (2018) 721–733. doi:10.1016/j.energy.2017.12.104.

[2] M. Alberdi -Pagola, S.E. Poulsen, R.L. Jensen, S. Madsen, Thermal response testing of precast pile heat exchangers: fieldwork report, Aalborg University, Aalborg, Denmark, 2017. http://vbn.aau.dk/files/266379225/Thermal_response_testing_of_precast_pile_heat_exchangers_fieldwork_report.pdf.

[3] F. Loveridge, W. Powrie, Temperature response functions (G-functions) for single pile heat exchangers, Energy. 57 (2013) 554–564. doi:http://dx.doi.org/10.1016/j.energy.2013.04.060.

[4] F. Loveridge, W. Powrie, G-Functions for multiple interacting pile heat exchangers, Energy. 64 (2014) 747–757. doi:http://dx.doi.org/10.1016/j.energy.2013.11.014.

[5] P. Eskilson, Thermal Analysis of Heat Extraction, University of Lund, Sweden, 1987.

[6] COMSOL Multiphysics, Introduction to COMSOL Multiphysics version 5.3, Burlington, 2017.

[7] S.L.A.M. Abdelaziz, Deep energy foundations: geotechnical challenges and design considerations, Virginia Polytechnic Institute and State University, Blacksburg, Virginia, 2013.

[8] E. Zanchini, S. Lazzari, Temperature distribution in a field of long Borehole Heat Exchangers (BHEs) subjected to a monthly averaged heat flux, Energy. 59 (2013) 570–580. doi:https://doi.org/10.1016/j.energy.2013.06.040.

[9] F. Loveridge, W. Powrie, 2D thermal resistance of pile heat exchangers, Geothermics. 50 (2014) 122–135. doi:http://dx.doi.org/10.1016/j.geothermics.2013.09.015.

[10] M. Alberdi-Pagola, R.L. Jensen, S. Madsen, S.E. Poulsen, Measurement of thermal properties of soil and concrete samples, Aalborg University, Aalborg, Denmark, 2017. http://vbn.aau.dk/files/266378485/Measurement_of_thermal_properties_of_soil_and_concrete_samples.pdf.

[11] R. Al-Khoury, Computational modeling of shallow geothermal systems, CRC Press, 2011.

[12] H.-J.G. Diersch, FEFLOW Finite Element Modeling of Flow, Mass and Heat Transport in Porous and Fractured Media, Springer Science & Business Media, 2014. doi:10.1007/978-3-642-38739-5.

[13] J.D. Spitler, M. Bernier, 2 - Vertical borehole ground heat exchanger design methods A2 - Rees, Simon J, in: Adv. Ground-Source Heat Pump Syst., Woodhead Publishing, 2016: pp.

29–61. doi:http://dx.doi.org/10.1016/B978-0-08-100311-4.00002-9.

[14] M. Cimmino, M. Bernier, F. Adams, A contribution towards the determination of g-functions using the finite line source, Appl. Therm. Eng. 51 (2013) 401–412. doi:http://dx.doi.org/10.1016/j.applthermaleng.2012.07.044.

[15] M. Cimmino, M. Bernier, A semi-analytical method to generate g-functions for geothermal bore fields, Int. J. Heat Mass Transf. 70 (2014) 641–650. doi:10.1016/j.ijheatmasstransfer.2013.11.037.

[16] M. Alberdi-Pagola, Thermal response test data of five quadratic cross section precast pile heat exchangers, Data Br. 18 (2018) 13–15. doi:10.1016/j.dib.2018.02.080.

[17] J. Doherty, PEST Model-Independent Parameter Estimation. User Manual, 5th Editio, 2010. file:///C:/Users/maap/Downloads/pestman.pdf.

Appendix

A) Curve fit results for ground temperature response functions: pile G-functions G_g

The ground temperature response G-functions for each AR are valid for 0.1 < Fo < 10000. G_g can be described as:

$$G_g = a \cdot \ln(Fo)^9 + b \cdot \ln(Fo)^8 + c \cdot \ln(Fo)^7 + d \cdot \ln(Fo)^6 + e \cdot \ln(Fo)^5 + f \cdot \ln(Fo)^4 + g \cdot \ln(Fo)^3 + h \cdot \ln(Fo)^2 + i \cdot \ln(Fo) + j \quad (11)$$

The curve fitting parameters are defined in Table 5. For Fo < 0.1, G_g should be set to zero.

Table 7: Curve fitting parameters for ground response factors G_g.

	AR = 15	AR = 30	AR = 45	AR = 53
a	4.04E-09	-6.133E-09	4.199E-09	4.938E-09
b	-6.28E-08	1.568E-07	-3.525E-08	-4.061E-08
c	-7.71E-07	-1.134E-06	-8.541E-07	-9.857E-07
d	1.31E-05	-2.850E-06	8.311E-06	8.874E-06
e	6.89E-05	1.151E-04	6.477E-05	7.218E-05
f	-1.06E-03	-7.257E-04	-8.423E-04	-8.504E-04
g	-4.70E-03	-4.868E-03	-3.519E-03	-3.562E-03
h	4.04E-02	4.514E-02	4.648E-02	4.713E-02
i	2.97E-01	3.243E-01	3.245E-01	3.272E-01
j	5.34E-01	5.689E-01	5.817E-01	5.854E-01
RMSE*	6.35E-06	1.138E-05	1.658E-05	1.665E-05
R^2**	9.999E-01	9.999E-01	9.999E-01	9.998E-01

*RMSE: Root Mean Squared Error
**R^2: Coefficient of Determination

B) Steady state concrete thermal resistance values R_c

The upper and lower bounds for the concrete thermal resistance R_c for square precast pile heat exchangers with single-U- and W-shape pipes for a range of thermal conductivities of concrete ($1 < \lambda_c < 4$) take the form:

$$R_c = a \cdot \lambda_c^5 + b \cdot \lambda_c^4 + c \cdot \lambda_c^3 + d \cdot \lambda_c^2 + e \cdot \lambda_c + f \quad (12)$$

The curve fitting parameters are defined in Table 6. Perform linear interpolation for non-computed values.

Table 8: Curve fitting parameters for upper and lower bounds for the concrete thermal resistance R_c.

	Single-U shape		W-shape	
λ_c/λ_s	**2**	**0.5**	**2**	**0.5**
a	-0.00255	-0.00151	-0.00105	-0.00096
b	0.03765	0.02234	0.01557	0.01422
c	-0.22166	-0.13312	-0.09284	-0.08438
d	0.66019	0.40771	0.28459	0.25660
e	-1.03559	-0.67667	-0.47303	-0.42066
f	0.79525	0.57674	0.40727	0.35237

C) Curve fit results for transient pile temperature response functions: concrete G-functions G_c

The transient concrete thermal resistance differs depending on the relation between the soil and the concrete, as shown in Figure 9.

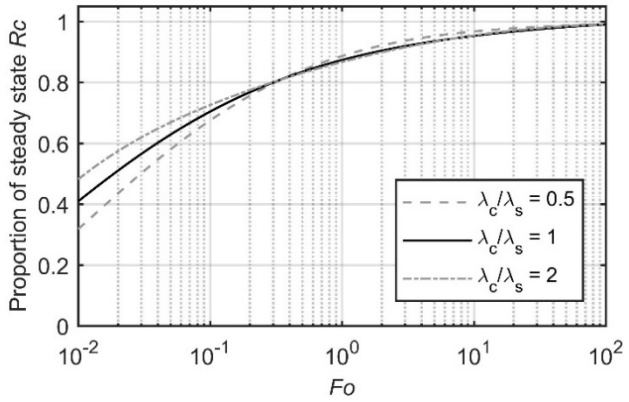

Figure 10: Proportion of steady state R_c for time of the W-shape pile heat exchanger and for different λ_c/λ_s ratios.

The concrete temperature response G-function G_c are valid for 0.01 < Fo < 100 and it takes the form:

$$G_c = a \cdot \ln(Fo)^6 + b \cdot \ln(Fo)^5 + c \cdot \ln(Fo)^4 + d \cdot \ln(Fo)^3 + e \cdot \ln(Fo)^2 + f \cdot \ln(Fo) + g \quad (13)$$

The curve fitting parameters are defined in Table 7. For Fo > 100 G_c should be set to 1 and for Fo < 0.01 G_c should be set to zero.

Table 9: Curve fitting parameters for concrete G-functions G_c.

	1U	2U		
λ_c/λ_s	**1**	**0.5**	**1**	**2**
a	1.7874E-06	7.4143E-07	3.2209E-06	-6.8329E-07
b	-9.9483E-06	-1.6587E-05	3.5142E-05	1.2454E-05
c	-1.5283E-04	6.6686E-05	-2.3294E-04	-4.7563E-05
d	1.9418E-03	1.0464E-03	-1.0900E-04	3.1674E-05
e	-9.8678E-03	-1.2676E-02	-5.0508E-03	-4.8439E-03
f	2.9573E-02	5.8398E-02	5.3798E-02	4.9111E-02
g	9.5364E-01	8.8640E-01	8.6614E-01	8.6694E-01
RMSE*	0.00032	0.0039	0.0025	0.00003
R^{2}**	0.99998	0.9991	0.9997	0.99992

*RMSE: Root Mean Squared Error
**R^2: Coefficient of Determination

D) Curve fit results for ground temperature response functions for distances

The ground temperature response G-functions for each distance are valid for min(Fo) < Fo < 10000. G_g can be described as:

$$G_g = a \cdot \ln(Fo)^9 + b \cdot \ln(Fo)^8 + c \cdot \ln(Fo)^7 + d \cdot \ln(Fo)^6 + e \cdot \ln(Fo)^5 + f \cdot \ln(Fo)^4 + g \cdot \ln(Fo)^3 + h \cdot \ln(Fo)^2 + i \cdot \ln(Fo) + j \quad (14)$$

The curve fitting parameters are defined in Table 8, 9, 10 and 11 for aspect ratios 15, 30, 45 and 50, respectively. For Fo < min(Fo), G_g should be set to zero.

Table 10: Spatial G-functions for AR 15.

S/2r	∞	1.3	2.0	2.6	5.2	7.8	8.4	10.5	12.6	13.1	16.7	19.6	26.2
Distance from pile edge [m]	0.00	0.50	0.75	1.00	2.00	3.00	3.20	4.00	4.80	5.00	6.40	7.50	10.00
a	4.04E-09	2.79E-09	-4.83E-09	-9.30E-09	-1.01E-08	-5.40E-09	-4.59E-09	-2.09E-09	-5.66E-10	-3.03E-10	6.97E-10	8.89E-10	7.16E-10
b	-6.28E-08	-1.22E-07	-4.22E-08	2.21E-08	9.75E-08	7.23E-08	6.56E-08	4.13E-08	2.35E-08	2.01E-08	4.40E-09	-1.10E-09	-4.25E-09
c	-7.71E-07	2.85E-07	1.57E-06	2.15E-06	1.74E-06	8.07E-07	6.65E-07	2.45E-07	9.48E-09	-2.91E-08	-1.63E-07	-1.77E-07	-1.27E-07
d	1.31E-05	2.11E-05	8.02E-06	-2.16E-06	-1.42E-05	-1.08E-05	-9.84E-06	-6.35E-06	-3.76E-06	-3.26E-06	-9.14E-07	-6.25E-08	4.92E-07
e	6.89E-05	-7.33E-05	-0.00015	-0.00018	-0.00012	-4.87E-05	-3.93E-05	-1.27E-05	1.34E-06	3.55E-06	1.07E-05	1.11E-05	7.63E-06
f	-1.06E-03	-1.39E-03	-6.71E-04	-1.26E-04	5.76E-04	4.77E-04	4.40E-04	2.98E-04	1.88E-04	1.66E-04	6.10E-05	2.03E-05	-1.12E-05
g	-4.70E-03	2.50E-03	5.06E-03	5.75E-03	3.77E-03	1.73E-03	1.45E-03	6.54E-04	2.17E-04	1.45E-04	-1.22E-04	-1.74E-04	-1.43E-04
h	4.04E-02	4.55E-02	3.02E-02	1.83E-02	-7.87E-04	-3.30E-03	-3.26E-03	-2.61E-03	-1.81E-03	-1.63E-03	-7.04E-04	-3.00E-04	5.20E-05
i	2.97E-01	1.03E-01	3.91E-02	8.33E-03	-1.61E-02	-1.03E-02	-9.01E-03	-4.83E-03	-2.19E-03	-1.72E-03	1.75E-04	6.69E-04	7.13E-04
j	5.34E-01	5.41E-02	0.004521	-0.0081	-0.00508	2.62E-04	7.53E-04	1.65E-03	1.66E-03	1.61E-03	1.06E-03	6.76E-04	1.78E-04
RMSE*	6.35E-06	1.60E-05	2.80E-05	2.33E-05	7.23E-06	6.09E-06	5.45E-06	3.95E-06	2.23E-06	1.95E-06	7.39E-07	3.30E-07	4.60E-08
R^{2}**	1.00E+00	9.99E-01	9.98E-01	9.99E-01	9.99E-01	9.45E-01	9.28E-01	9.81E-01	9.92E-01	9.66E-01	1.00E+00	9.87E-01	9.93E-01
min Fo [-]	0.01	0.46	0.95	2.10	9.00	20.00	20.00	33.50	41.00	58.00	100.00	115.00	175.00
min time [h]	0.10	4.66	9.63	21.28	91.20	202.67	202.67	339.48	415.48	587.75	1013.36	1165.37	1773.38
max Phi	2.33	1.44	1.13	0.92	0.49	0.30	0.28	0.20	0.15	0.14	0.09	0.06	0.03
max Fo	10000	10000	10000	10000	10000	10000	10000	10000	10000	10000	10000	10000	10000

*RMSE: Root Mean Squared Error

**R^2: Coefficient of Determination

Table 11: Spatial G-functions for AR 30.

S/2r	∞	1.3	2.0	2.6	5.2	7.8	10.5	13.1	15.6	19.6	23.4	26.2	31.2
Distance from pile edge [m]	0.00	0.50	0.75	1.00	2.00	3.00	4.00	5.00	5.95	7.50	8.93	10.00	11.90
a	-6.133E-09	1.592E-08	1.462E-08	3.032E-09	-3.090E-08	-2.950E-08	-1.835E-08	-8.193E-09	-1.423E-09	4.478E-09	6.338E-09	6.524E-09	5.694E-09
b	1.568E-07	-3.884E-07	-4.648E-07	-2.610E-07	5.431E-07	6.249E-07	4.464E-07	2.521E-07	1.103E-07	-2.753E-08	-8.293E-08	-9.809E-08	-9.627E-08
c	-1.134E-06	1.065E-06	3.224E-06	3.712E-06	1.042E-06	-8.417E-07	-1.408E-06	-1.386E-06	-1.177E-06	-7.791E-07	-4.822E-07	-3.166E-07	-1.265E-07
d	-2.850E-06	3.737E-05	3.045E-05	8.788E-06	-4.946E-05	-4.916E-05	-3.272E-05	-1.717E-05	-6.483E-06	3.368E-06	7.014E-06	7.845E-06	7.355E-06
e	1.151E-04	-1.932E-04	-3.436E-04	-3.290E-04	6.678E-06	1.488E-04	1.576E-04	1.253E-04	8.948E-05	4.287E-05	1.593E-05	3.510E-06	-7.582E-06
f	-7.257E-04	-1.620E-03	-8.398E-04	1.088E-05	1.501E-03	1.312E-03	8.230E-04	4.161E-04	1.529E-04	-7.755E-05	-1.577E-04	-1.739E-04	-1.598E-04
g	-4.868E-03	6.314E-03	1.010E-02	9.692E-03	1.601E-03	-2.005E-03	-2.544E-03	-2.093E-03	-1.493E-03	-6.775E-04	-2.039E-04	1.077E-05	1.941E-04
h	4.514E-02	5.190E-02	3.323E-02	1.794E-02	-6.802E-03	-8.278E-03	-5.495E-03	-2.838E-03	-1.079E-03	4.586E-04	9.856E-04	1.090E-03	9.959E-04
i	3.243E-01	9.452E-02	2.136E-02	-5.962E-03	-5.438E-03	6.321E-03	8.970E-03	7.734E-03	5.664E-03	2.646E-03	8.179E-04	-2.910E-05	-7.663E-04
j	5.689E-01	5.337E-02	1.583E-03	-8.649E-03	2.333E-03	7.817E-03	6.984E-03	4.715E-03	2.745E-03	5.910E-04	-4.216E-04	-7.884E-04	-9.730E-04
RMSE*	1.138E-05	9.286E-06	8.246E-06	8.402E-06	6.814E-06	5.272E-06	5.359E-06	5.164E-06	4.005E-06	1.858E-06	7.265E-07	3.368E-07	1.107E-07
R^2**	1.000E+00	9.997E-01	9.997E-01	9.999E-01	9.992E-01	9.999E-01	1.000E+00	1.000E+00	9.998E-01	1.000E+00	9.999E-01	1.000E+00	9.998E-01
min Fo [-]	0.01	0.43	0.95	2.10	8.00	20.00	26.00	33.50	41.00	58.00	100.00	115.00	175.00
min time [h]	0.10	4.36	9.63	21.28	81.07	202.67	263.47	339.48	415.48	587.75	1013.36	1165.37	1773.38
max Phi	3.07	2.07	1.71	1.46	0.92	0.65	0.48	0.37	0.29	0.21	0.15	0.12	0.09
max Fo	10000	10000	10000	10000	10000	10000	10000	10000	10000	10000	10000	10000	10000

*RMSE: Root Mean Squared Error
**R^2: Coefficient of Determination

Table 12: Spatial G-functions for AR 45.

$S/2r_b$	∞	1.3	2.0	2.6	5.2	7.9	10.5	13.1	19.6	22.8	26.2	34.2	45.6
Distance from pile edge [m]	0.00	0.50	0.75	1.00	2.00	3.00	4.00	5.00	7.50	8.70	10.00	13.05	17.40
a	4.199E-09	2.392E-09	-5.884E-09	-1.052E-08	-9.248E-09	-1.870E-09	3.169E-09	5.693E-09	6.248E-09	5.406E-09	4.353E-09	2.246E-09	6.536E-10
b	-3.525E-08	-9.048E-08	-3.823E-10	7.076E-08	1.389E-07	8.660E-08	3.149E-08	-5.976E-09	-4.042E-08	-4.138E-08	-3.801E-08	-2.521E-08	-1.085E-08
c	-8.541E-07	3.281E-07	1.694E-06	2.267E-06	1.404E-06	1.246E-08	-8.020E-07	-1.156E-06	-1.115E-06	-9.385E-07	-7.394E-07	-3.666E-07	-1.007E-07
d	8.311E-06	1.546E-05	6.875E-07	-1.062E-05	-2.182E-05	-1.446E-05	-6.407E-06	-7.995E-07	4.745E-06	5.122E-06	4.852E-06	3.348E-06	1.493E-06
e	6.477E-05	-8.856E-05	-1.714E-04	-1.926E-04	-9.560E-05	2.152E-06	5.308E-05	7.320E-05	6.764E-05	5.643E-05	4.419E-05	2.190E-05	6.226E-06
f	-8.423E-04	-1.116E-03	-2.979E-04	3.158E-04	1.021E-03	7.615E-04	4.225E-04	1.714E-04	-1.086E-04	-1.435E-04	-1.492E-04	-1.130E-04	-5.328E-05
g	-3.519E-03	4.209E-03	6.877E-03	7.437E-03	4.321E-03	1.341E-03	-2.729E-04	-1.015E-03	-1.256E-03	-1.092E-03	-8.816E-04	-4.597E-04	-1.418E-04
h	4.648E-02	4.981E-02	3.187E-02	1.806E-02	-4.088E-03	-6.134E-03	-4.251E-03	-2.209E-03	5.635E-04	1.016E-03	1.179E-03	9.919E-04	4.997E-04
i	3.245E-01	1.100E-01	3.877E-02	4.341E-03	-2.050E-02	-1.030E-02	-1.528E-03	3.378E-03	6.238E-03	5.696E-03	4.760E-03	2.627E-03	8.745E-04
j	5.817E-01	6.060E-02	5.990E-03	-7.559E-03	-2.580E-03	3.802E-03	4.919E-03	4.112E-03	1.336E-03	4.792E-04	-1.042E-04	-5.966E-04	-4.694E-04
RMSE*	1.658E-05	1.609E-05	2.035E-05	1.374E-05	1.418E-05	1.943E-05	1.491E-05	9.313E-06	2.111E-06	1.382E-06	1.152E-06	8.269E-07	3.081E-07
R^{2}**	9.999E-01	1.000E+00	1.000E+00	1.000E+00	1.000E+00	9.998E-01	1.000E+00	9.997E-01	9.971E-01	9.894E-01	9.925E-01	9.962E-01	9.972E-01
min Fo [-]	0.01	0.43	0.85	1.7	10	20	25	32	78	115	155	240	350
min time [h]	0.10	4.36	8.61	17.23	101.34	202.67	253.34	324.28	790.42	1165.37	1570.71	2432.07	3546.76
max Phi	3.45	2.43	2.05	1.79	1.21	0.90	0.70	0.56	0.35	0.28	0.22	0.14	0.06
max Fo	10000	10000	10000	10000	10000	10000	10000	10000	10000	10000	10000	10000	10000

*RMSE: Root Mean Squared Error
**R^2: Coefficient of Determination

Table 13: Spatial G-functions for AR 53.

B/2r	∞	1.31	1.96	2.62	5.24	7.85	10.47	13.09	19.63	26.96	26.18	40.45	53.93
Distance from pile edge [m]	0.00	0.50	0.75	1.00	2.00	3.00	4.00	5.00	7.50	10.30	10.00	15.45	20.60
a	4.938E-09	3.084E-09	-5.240E-09	-9.889E-09	-8.448E-09	-8.617E-10	4.286E-09	6.818E-09	7.137E-09	4.909E-09	4.632E-09	1.265E-09	1.785E-10
b	-4.061E-08	-9.555E-08	-4.755E-09	6.688E-08	1.343E-07	7.969E-08	2.257E-08	-1.607E-08	-5.046E-08	-4.597E-08	-4.457E-08	-1.958E-08	-5.788E-09
c	-9.857E-07	2.068E-07	1.579E-06	2.151E-06	1.250E-06	-1.756E-07	-1.004E-06	-1.354E-06	-1.264E-06	-8.295E-07	-7.793E-07	-1.984E-07	-2.413E-08
d	8.874E-06	1.597E-05	1.083E-06	-1.030E-05	-2.142E-05	-1.371E-05	-5.342E-06	4.615E-07	6.067E-06	5.932E-06	5.778E-06	2.681E-06	8.227E-07
e	7.218E-05	-8.203E-05	-1.651E-04	-1.860E-04	-8.600E-05	1.404E-05	6.576E-05	8.556E-05	7.692E-05	4.987E-05	4.683E-05	1.227E-05	1.784E-06
f	-8.504E-04	-1.121E-03	-2.961E-04	3.226E-04	1.027E-03	7.525E-04	3.989E-04	1.374E-04	-1.508E-04	-1.859E-04	-1.834E-04	-9.448E-05	-3.024E-05
g	-3.562E-03	4.206E-03	6.882E-03	7.431E-03	4.215E-03	1.155E-03	-4.981E-04	-1.249E-03	-1.447E-03	-1.006E-03	-9.500E-04	-2.750E-04	-4.904E-05
h	4.713E-02	5.039E-02	3.226E-02	1.831E-02	-4.099E-03	-6.096E-03	-4.100E-03	-1.959E-03	9.196E-04	1.508E-03	1.508E-03	8.739E-04	2.945E-04
i	3.272E-01	1.113E-01	3.954E-02	4.817E-03	-2.004E-02	-9.465E-03	-4.331E-04	4.580E-03	7.300E-03	5.489E-03	5.220E-03	1.667E-03	3.426E-04
j	5.854E-01	6.101E-02	5.999E-03	-7.650E-03	-2.495E-03	3.967E-03	5.036E-03	4.137E-03	1.166E-03	-3.514E-04	-4.481E-04	-7.647E-04	-3.388E-04
RMSE*	1.665E-05	1.766E-05	2.274E-05	1.554E-05	1.423E-05	1.877E-05	1.419E-05	8.605E-06	2.254E-06	1.740E-06	1.831E-06	8.595E-07	1.460E-07
R^{2}**	9.998E-01	1.000E+00	1.000E+00	1.000E+00	1.000E+00	9.998E-01	9.999E-01	9.989E-01	9.973E-01	9.943E-01	9.964E-01	9.969E-01	9.954E-01
min Fo [-]	0.02	0.50	1.00	2.00	10.00	20.00	30.00	40.00	115.00	180.00	220.00	350.00	400.00
min time [h]	0.20	5.07	10.13	20.26	101.32	202.64	303.96	405.28	1165.19	1823.78	2229.07	3546.24	4052.85
max Phi	3.61	2.58	2.20	1.94	1.34	1.02	0.81	0.66	0.42	0.28	0.27	0.12	0.04
max Fo	10000	10000	10000	10000	10000	10000	10000	10000	10000	10000	10000	10000	10000

*RMSE: Root Mean Squared Error
**R^{2}: Coefficient of Determination